CrossMark click for updates

Network architecture of the cerebral nuclei (basal ganglia) association and commissural connectome

Larry W. Swanson[a,1], Olaf Sporns[b], and Joel D. Hahn[a]

[a]Department of Biological Sciences, University of Southern California, Los Angeles, CA 90089; and [b]Department of Psychological and Brain Sciences, Indiana University, Bloomington, IN 47405

Contributed by Larry W. Swanson, August 10, 2016 (sent for review July 18, 2016; reviewed by Ann M. Graybiel and Liqun Luo)

The cerebral nuclei form the ventral division of the cerebral hemisphere and are thought to play an important role in neural systems controlling somatic movement and motivation. Network analysis was used to define global architectural features of intrinsic cerebral nuclei circuitry in one hemisphere (association connections) and between hemispheres (commissural connections). The analysis was based on more than 4,000 reports of histologically defined axonal connections involving all 45 gray matter regions of the rat cerebral nuclei and revealed the existence of four asymmetrically interconnected modules. The modules form four topographically distinct longitudinal columns that only partly correspond to previous interpretations of cerebral nuclei structure–function organization. The network of connections within and between modules in one hemisphere or the other is quite dense (about 40% of all possible connections), whereas the network of connections between hemispheres is weak and sparse (only about 5% of all possible connections). Particularly highly interconnected regions (rich club and hubs within it) form a topologically continuous band extending through two of the modules. Connection path lengths among numerous pairs of regions, and among some of the network's modules, are relatively long, thus accounting for low global efficiency in network communication. These results provide a starting point for reexamining the connectional organization of the cerebral hemispheres as a whole (right and left cerebral cortex and cerebral nuclei together) and their relation to the rest of the nervous system.

behavior | connectomics | mammal | neural connections | neuroinformatics

The paired adult vertebrate cerebral hemispheres are differentiations of the embryonic neural tube's endbrain (telencephalic) vesicle, which in turn forms a ventral nonlaminated part, the cerebral nuclei, and then a dorsal laminated part, the cerebral cortex (1–3). In mammals the largest parts of the cerebral nuclei by volume are the caudoputamen (striatal) and globus pallidus (pallidal). Together, they are commonly regarded as the endbrain parts of the basal ganglia (3), which play an important role in controlling skeletomuscular (somatic) movements and in the etiology of movement disorders (4).

A major shift in thinking about the basal ganglia occurred with the recognition that certain ventral parts of the cerebral nuclei display the same basic circuit organization, but involve different parts of a cerebral cortex to cerebral nuclei to thalamus to cerebral cortex loop (5). This finding led to an expanded view of the basal ganglia, with dorsal and ventral striatopallidal subsystems involved primarily in movement (dorsal) and motivational functionality (ventral) (6). Complete expansion of the view was then proposed on the basis of connectional, gene expression, embryological, and functional evidence (7). It was hypothesized that the entire cerebral cortex, cerebral nuclei, and thalamus can be divided into four basic subsystems involving dorsal, ventral, medial, and caudorostral domains of the striatopallidum.

The present study reexamines the organization of axonal connections between all parts of the cerebral nuclei, using systematic, data-driven, network analysis methods (8, 9). The analysis is based on a directed, weighted macroconnectome of association connections (between ipsilateral parts) and commissural connections (between parts on one side and those on the other side), using the same basic strategy and methodology applied to the rat cerebral cortical association macroconnectome (10) but with additional analytical approaches and curation tools. In this approach a macroconnection is defined as a monosynaptic axonal (directed, from/to) connection between two nervous system gray matter regions or between a gray matter region and another part of the body (such as a muscle) (11, 12). All 45 gray matter regions of the cerebral nuclei on each side of the brain were included in the analysis. The goal of this analysis was to provide global, high-level, design principles of intrinsic cerebral nuclei circuitry as a framework for more detailed research at the meso-, micro-, and nanolevels of analysis (13).

Results

Systematic curation of the primary neuroanatomical literature yielded no reports of statistically significant male/female, right/left, or strain differences for any association or commissural connection used in the analysis, which therefore simply applies to the adult rat in the absence of further data. The entire dataset was derived from 4,067 connection reports expertly curated from 40 peer-reviewed original research articles; 2,731 or 67.2% of the connection reports were from the L.W.S. laboratory. A standard rat brain atlas nomenclature (Dataset S1) was used to describe all connection reports (Dataset S2), which were based on a variety of experimental monosynaptic anterograde and retrograde axonal pathway tracing methods identified for each connection report in Dataset S2.

Single-Hemisphere Connection Number. The curation identified 731 rat cerebral nuclei association macroconnections (RCNAMs) as present and 1,051 as absent, between the 45 gray matter regions analyzed for the cerebral nuclei as a whole; this result yields a connection density of 41% (731/1,782). No adequate published

Significance

The cerebral nuclei together with the cerebral cortex form the cerebral hemispheres that are critically important for the control of voluntary behavior and motivation. Network analysis of microscopic connectional data collected since the 1970s in a small, intensely studied mammal provides a new way to understand overall design features of circuitry coordinating activity in the various parts of the cerebral nuclei on both sides of the brain. Basically, intracerebral nuclei circuitry is organized into four modules on each side of the brain, with connections within and between modules on one side being quite dense and connections between the cerebral nuclei on either side being quite sparse. The results provide insight into cerebral nuclei structure and function.

Author contributions: L.W.S. designed research; L.W.S. and O.S. performed research; O.S. and J.D.H. contributed new reagents/analytic tools; O.S. analyzed data; and L.W.S. wrote the paper.

Reviewers: A.M.G., Massachusetts Institute of Technology; and L.L., Stanford University.

The authors declare no conflict of interest.

Data deposition: Network analysis tools are available at the Brain Connectivity Toolbox.

[1]To whom correspondence should be addressed. Email: larryswanson10@gmail.com.

This article contains supporting information online at www.pnas.org/lookup/suppl/doi:10.1073/pnas.1613184113/-/DCSupplemental.

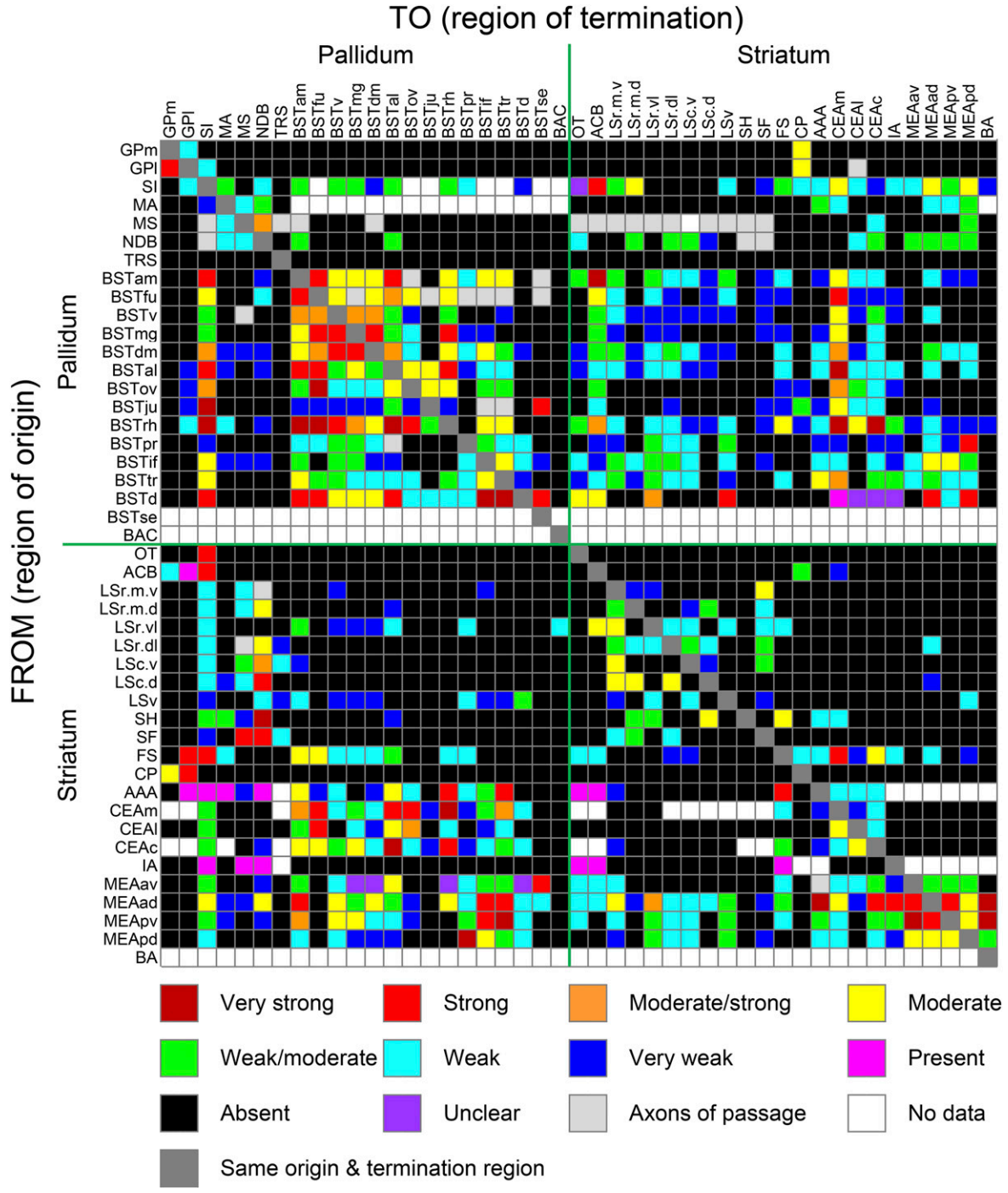

Fig. 1. Rat cerebral nuclei association connectome. Directed synaptic macroconnection matrix with gray matter region sequence in the topographically ordered nomenclature hierarchy is provided in Dataset S1. Color scale of connection weights and properties is at the bottom. Abbreviations: AAA, anterior amygdalar area; ACB, accumbens nucleus; BA, bed nucleus of accessory olfactory tract; BAC, bed nucleus of anterior commissure; BSTal, anterolateral area of bed nuclei of terminal stria; BSTam, anteromedial area of bed nuclei of terminal stria; BSTd, dorsal nucleus of bed nuclei of terminal stria; BSTdm, dorsomedial nucleus of bed nuclei of terminal stria; BSTfu, fusiform nucleus of bed nuclei of terminal stria; BSTif, interfascicular nucleus of bed nuclei of terminal stria; BSTju, juxtacapsular nucleus of bed nuclei of terminal stria; BSTmg, magnocellular nucleus of bed nuclei of terminal stria; BSTov, oval nucleus of bed nuclei of terminal stria; BSTpr, principal nucleus of bed nuclei of terminal stria; BSTrh, rhomboid nucleus of bed nuclei of terminal stria; BSTse, strial extension of bed nuclei of terminal stria; BSTtr, transverse nucleus of bed nuclei of terminal stria; BSTv, ventral nucleus of bed nuclei of terminal stria; CEAc, capsular part of central amygdalar nucleus; CEAl, lateral part of central amygdalar nucleus; CEAm, medial part of central amygdalar nucleus; CP, caudoputamen; FS, striatal fundus; GPl, lateral globus pallidus; GPm, medial globus pallidus; IA, intercalated amygdalar nuclei; LSc.d, dorsal zone of caudal part of lateral septal nucleus; LSc.v, ventral zone of caudal part of lateral septal nucleus; LSr.dl, dorsolateral zone of rostral part of lateral septal nucleus; LSr.m.d, dorsal region of medial zone of rostral part of lateral septal nucleus; LSr.m.v, ventral region of medial zone of rostral part of lateral septal nucleus; LSr.vl, ventrolateral zone of rostral part of lateral septal nucleus; LSv, ventral part of lateral septal nucleus; MA, magnocellular nucleus; MEAad, anterodorsal part of medial amygdalar nucleus; MEAav, anteroventral part of medial amygdalar nucleus; MEApd, posterodorsal part of medial amygdalar nucleus; MEApv, posteroventral part of medial amygdalar nucleus; MS, medial septal nucleus; NDB, diagonal band nucleus; OT, olfactory tubercle; SF, septofimbrial nucleus; SH, septohippocampal nucleus; SI, innominate substance; TRS, triangular septal nucleus.

data were found for 198 (10.0%) of all 1,980 ($45^2 - 45$) possible association macroconnections; this result yields a matrix coverage (fill ratio) of 90% (Fig. 1). Assuming the curated literature representatively samples the 45-region matrix, the complete RCNAM dataset would contain ~812 macroconnections (1,980 × 0.41), with a projected average of 18 input/output association macroconnections per cerebral nuclei region (812/45). For network analysis, values of "unclear" and "no data" are assigned to and combined with values in the "absent" category, resulting in a connection density of 37% (731/1,980). Considering only connections that have been unambiguously identified yields an average of input/output macroconnections of 16.2 (731/45), with significant variations for particular cerebral nuclei regions (input range 1–38, output range 0–36; Fig. 2 *A* and *B*). Individual regions show large variations in the ratio of the number of distinct inputs and outputs (their in degree and their out degree; Fig. 2*A*) as well as the aggregated strength of these inputs and outputs (their in strength and their out strength; Fig. 2*B*). Strong imbalance implies that some regions specialize as "receivers" of inputs and others as "senders" of outputs. The distribution of weight categories for the 731 connections reported as present is shown in Fig. S1*A*. The weight scale used for weighted network analysis is shown in Fig. S1*B*.

Network Analysis for Modules. For single-hemisphere interconnections, modules were detected by modularity maximization while systematically varying a spatial resolution parameter γ to assess module stability (9, 14). Varying γ within the interval [0.5–1.5] centered on the default setting of γ = 1 resulted in four stable solutions (Fig. 3) with four to seven modules each. One module (M4) was stable across the entire range of γ, whereas modules M1–M3 were stable across most of the range. As the resolution parameter was increased toward finer and finer partitions, M3 split into two and then three submodules. The four-module solution was stable over the broadest range of γ and had the largest ratio of within-to-between module connection density in the range of γ examined here; hence, it was chosen for further analysis. The four-module solution with all regions and connections can be displayed as a weighted matrix (Fig. 4) or as a spring-embedded layout (Fig. 5*A*), and the regional composition of each module is provided in Fig. S2.

Connection Patterns. The simplest way to view the between-module interaction pattern is with aggregated between-module connections (Fig. 5*B*), which show that M1 and M3 are predominantly sending modules, M2 is predominantly a receiving module, and M4 is only weakly connected with the other modules. There are at least weak bidirectional connections between all four modules.

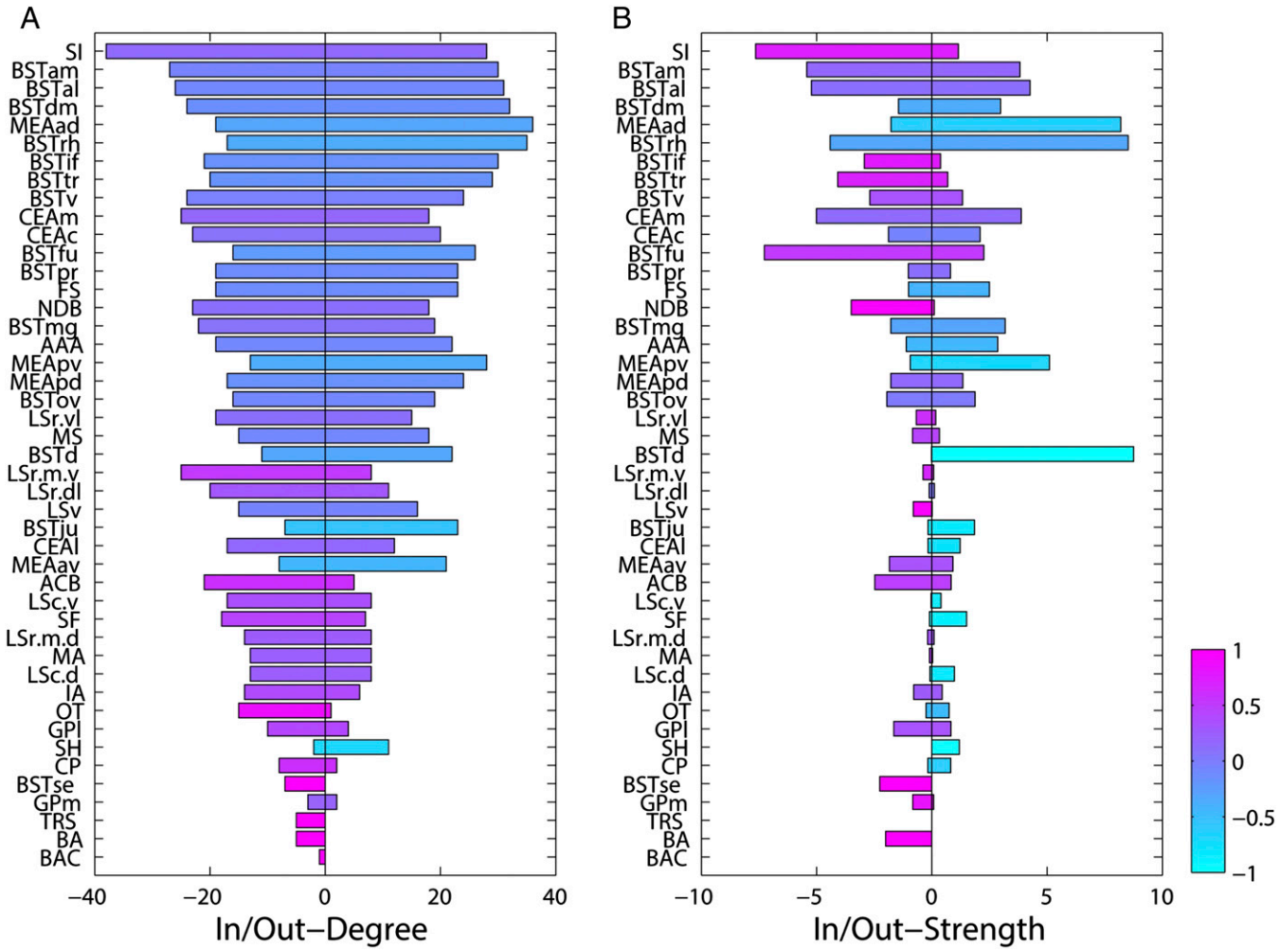

Fig. 2. (*A* and *B*) In degree/out degree (*A*) and in strength/out strength (*B*) for all regions of the single-hemisphere rat cerebral nuclei association macroconnection network. Regions are ranked by total degree, in descending order. Bar colors indicate the asymmetry in in/out degree and in/out strength, respectively, computed as (in degree – out degree)/(in degree + out degree) and (in strength – out strength)/(in strength + out strength). A value of −1 (cyan) indicates strong prevalence of out degree/strength (the area is a "sender") and a value of +1 (magenta) indicates a strong prevalence of in degree/strength (the area is a "receiver"). For abbreviations see Fig. 1.

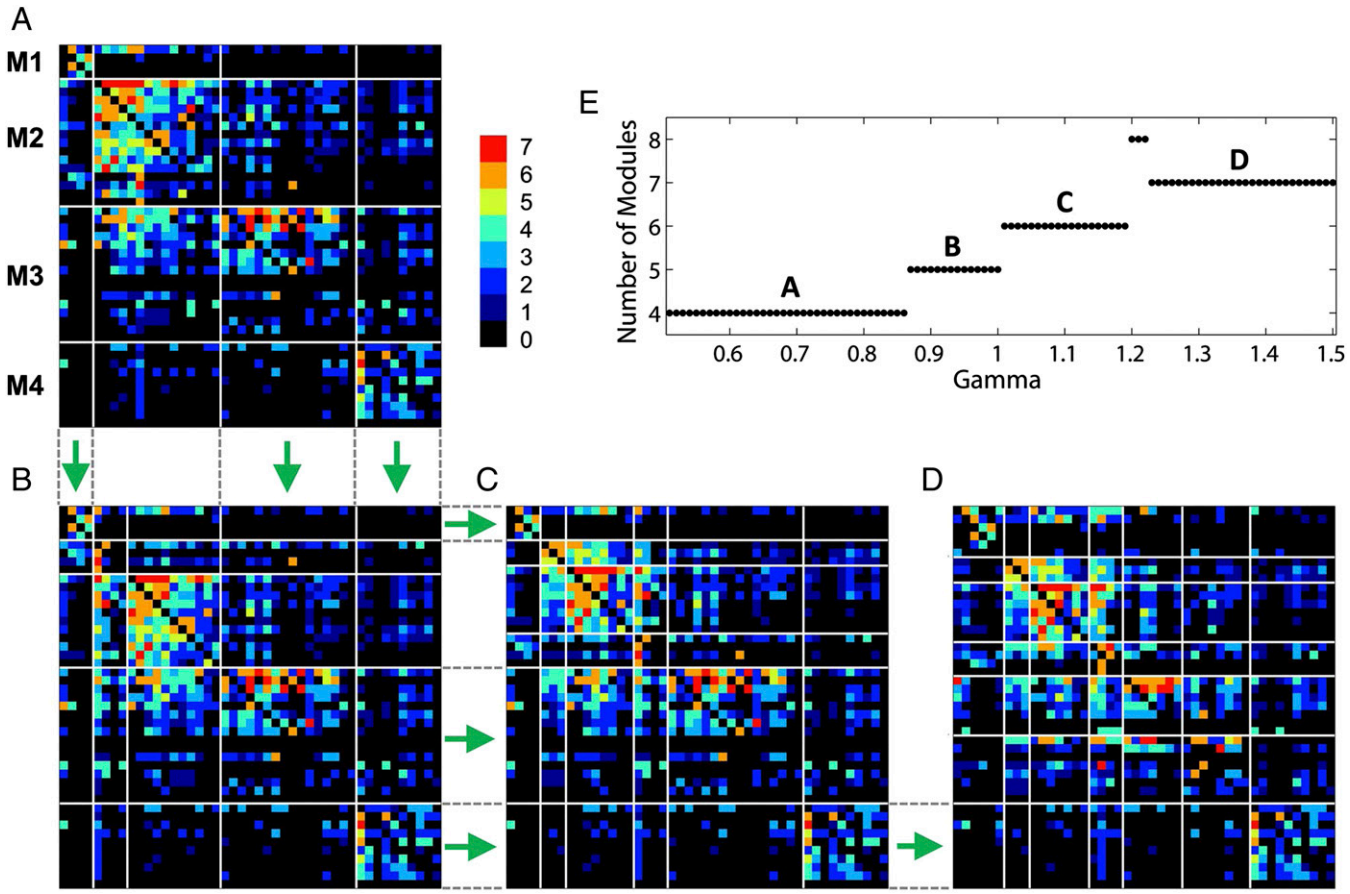

Fig. 3. Stability of module partitions under variation of spatial resolution parameter γ. *A–D* show four stable module partitions encountered in the range γ = [0.5–1.5], with regions within modules arranged by their total node strength. *E* plots the number of modules encountered at each level of γ. All four partitions shown here remain stable across their respective ranges of γ, as verified by computing the variation of information across partitions. Green arrows between *A–D* indicate modules that remain unchanged across different solutions. Note that M4 is robustly detected at all levels of γ. An unstable solution encountered around γ = 1.2 is excluded from the analysis. The four-module solution (*A*) is adopted in the remainder of the study. Region abbreviations along the axes for *A* are provided in the same sequence as in Fig. 4 and are defined in the legend of Fig. 1. The color scale refers to the seven weight categories (1, very weak; 2, weak; 3, weak to moderate; 4, moderate; 5, moderate to strong; 6, strong; 7, very strong) of existing connections, and 0 corresponds to connections that are shown to be absent or for which there are no data.

Corresponding average module-by-module connection densities (binary and weighted) further illustrate this point and are provided in Table S1. Table S2 lists counts and percentages of connection classes by matrix block. Strongly asymmetric average connection weights between modules result in strongly directed (asymmetric) connection patterns among modules.

The weighted RCNAM network can be decomposed into a symmetric (fully reciprocated) and a directed (fully nonreciprocated) component (15). To quantify the extent to which the distribution of connection weights in the RCNAM network is asymmetric, we computed the network's reciprocity ρ, a quantity that was then scaled with respect to a degree-preserving randomized null model. The reciprocity of the RCNAM network is ρ = 0.262, which indicates a tendency to reciprocate that is less strong than that of the network of rat cortical association macroconnections (RCAMs) that yields ρ = 0.331.

The 45 regions of the RCNAM network comprise striatal (23 regions) and pallidal (22 regions) parts (Fig. 1). Whereas connections from pallidal to striatal regions are denser (45%) than striatal to pallidal connections (33%), the aggregated weight of striatal to pallidal connections is twice as strong as for the reverse direction. Stronger striatal to pallidal connections are also encountered within each of the four modules.

Efficiency, Hubs, and Rich Club. The overall network topology does not display classic small-world attributes, which is due to its relatively long path length (resulting in relatively low efficiency). Whereas clustering is greater than in randomized controls, the network is also significantly less efficient [clustering coefficient (CC) = 0.0189 ($0.0108 \pm 7.35 \times 10^{-4}$; mean and SD of a population of random networks that were globally rewired while preserving the degree sequence (*SI Materials and Methods*); global efficiency (GE) = 0.0837 (0.1351 ± 0.0104)]. This trend prevails when nodes that lack identified association outputs [triangular septal nucleus (TRS), strial extension of bed nuclei of terminal stria (BSTse), bed nucleus of anterior commissure (BAC), and bed nucleus of accessory olfactory tract (BA)] are removed from the matrix [CC = 0.0179 ($0.0109 \pm 5.48 \times 10^{-4}$), GE = 0.0959 ($0.1512 \pm 0.0116$)]. The low efficiency of the RCNAM network is due to the existence of long paths between many of the networks' regions and modules. Whereas the mean path length between region pairs is 3.16 steps (computed from the weighted RCNAM network), 75 region pairs are linked by a minimal path with a length of 6 steps or greater. Among module pairs, modules M1 and M4 are topologically most distant from each other (see Fig. 5*A*) and are separated by, on average, 4.9 (M4 → M1) and 4.6 (M1 → M4) steps.

Centrality measures (degree, strength, betweenness, closeness) are summarized in Fig. S3. Regions innominate substance (SI), anteromedial area of bed nuclei of terminal stria (BSTam), anterolateral area of bed nuclei of terminal stria (BSTal), rhomboid nucleus of bed nuclei of terminal stria (BSTrh) and anterodorsal part of medial amygdalar nucleus (MEAad) (abbreviations in Fig. 1) rank in the top 20th percentile on all four measures, thus forming

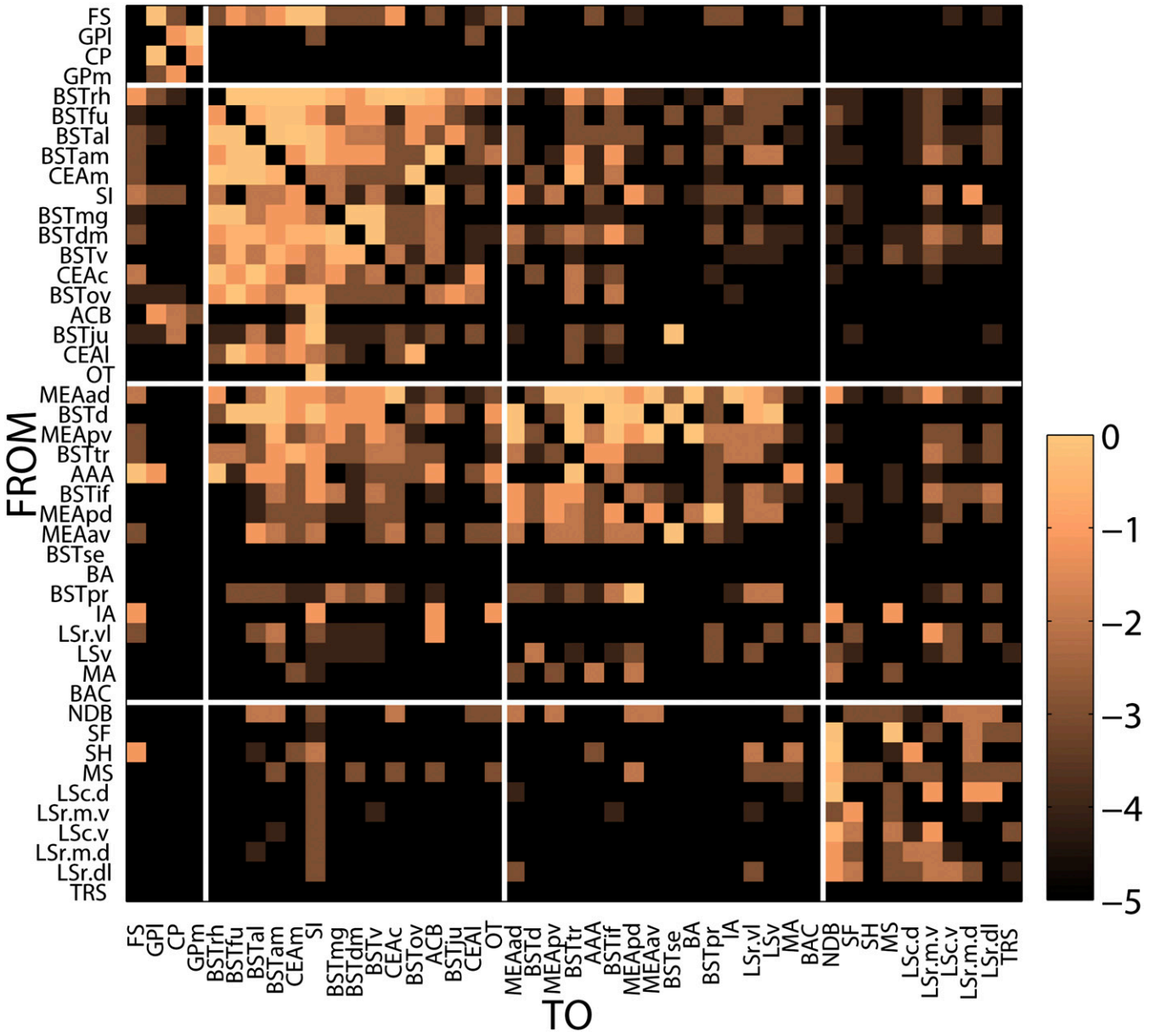

Fig. 4. Weighted connection matrix ($\log_{10}$ scale) for 45 (single-hemisphere) areas. Ordering is as for the four-module matrix in Fig. 3*A*, with regions within modules arranged by total node strength. For abbreviations see Fig. 1.

putative hubs in the association network topology. These five regions form a fully connected subgraph with an average connection weight of 0.39 (compared with a density of 37% and an average connection weight of 0.04 for the entire network). Four of the five candidate hubs are located in M2, with a sole hub (MEAad) in M3.

Rich club organization is present, as indicated by significantly greater density of connections among high-degree nodes compared with that in a degree-sequence–preserving null model (Fig. S4). Significance was assessed after correcting *P* values for multiple comparisons. The rich club shell where the corrected *P* value was minimal ($P = 3 \times 10^{-7}$) contains nine member regions, including the five putative hubs listed above: SI, BSTam, ventral nucleus of bed nuclei of terminal stria (BSTv), dorsomedial nucleus of bed nuclei of terminal stria (BSTdm), BSTal, BSTrh, interfascicular nucleus of bed nuclei of terminal stria (BSTif), transverse nucleus of bed nuclei of terminal stria (BSTtr), and MEAad. Rich club members overlap exclusively with modules M2 and M3.

Topographic Arrangement of Modules, Rich Club, and Hubs. The spatial distribution of the four modules and their 45 individual regional components was mapped onto a standard brain atlas (16) to distinguish whether module components are topographically either interdigitated or segregated (Fig. 6). Clearly, the modules form four spatially segregated longitudinal columns that may be described as dorsal (M1), ventral (M2), medial (M4), and rostrocaudal (M3), the latter of which consists of two segments (rostral and caudal) separated by a gap formed by region SI. The rich club also forms a spatially segregated mass of regions in M2 and M3 (Fig. 6), with the putative hubs nested within it.

The dorsal module (M1) corresponds to the classic dorsal striatopallidal system (3, 4), whereas the ventral module (M2) includes the classic ventral striatopallidum (5) and the central amygdalar nucleus and anterior division of bed nuclei of terminal stria (17). The caudal segment of M3 is formed by the medial amygdalar nucleus (striatal) and related regions, whereas the rostral segment is formed by the posterior division of bed nuclei

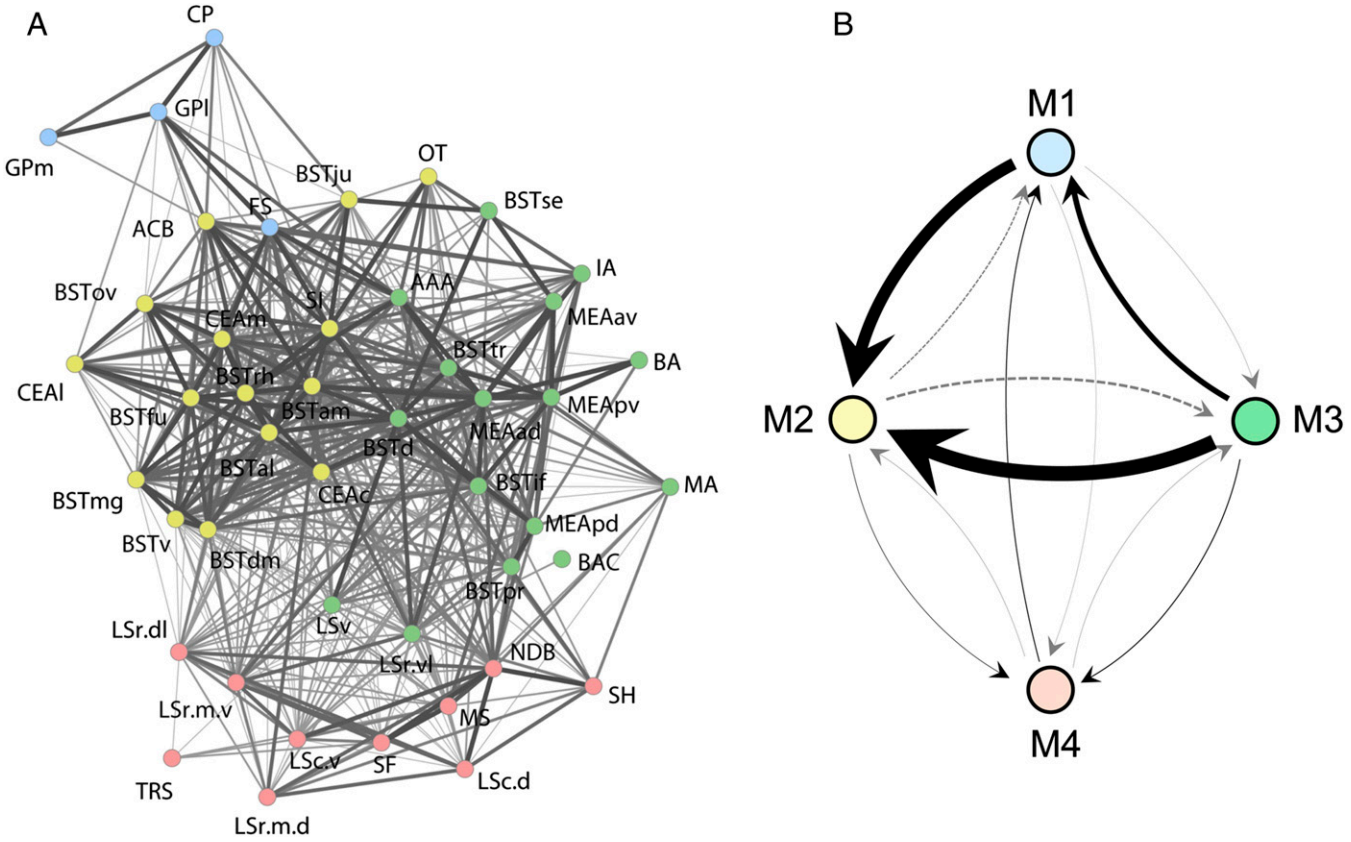

Fig. 5. Layout diagrams of connection patterns in a single hemisphere. (*A*) Nodes (regions) and edges (connections) are projected onto two dimensions, using a Fruchterman–Reingold energy minimization layout algorithm. Nodes are color coded by module assignment (M1, blue; M2, yellow; M3, green; M4, red). To simplify the plot, connections are drawn without reference to directionality (gray color level and thickness of line proportional to $\log_{10}$ of connection weight). (*B*) Summary layout of aggregated connection weights between modules M1–M4. Arrows show directionality of connections and their thickness is proportional to the average connection weights of between-module connections. For abbreviations see Fig. 1.

of terminal stria (pallidal) and adjacent ventral parts of the lateral septal nucleus (17). Finally, the medial module (M4) consists of the bulk of the septal region, which has both striatal and pallidal components (7, 18).

Connections Between Hemispheres. Curation identified 96 commissural connections as present and 1,693 as absent (that is, of 1,789 connections for which adequate data were available, 5.4% are present, indicating a relatively sparse commissural network) between the 45 gray matter regions analyzed for all cerebral nuclei in each hemisphere. No adequate published data were found for 236 (11.7%) of all 2,025 (45^2) possible commissural macroconnections, for a matrix coverage of 88.3%. Assuming the curated literature representatively samples the 45-region matrix, the complete rat cerebral nuclei commissural macroconnectome (RCNCM) dataset would contain ~109 macroconnections (2,025 × 0.054), with an average of 2.4 output commissural macroconnections per cerebral nuclei region (109/45). The matrix of identified projections has a density of 96/2,025 (4.7%). Whereas this density corresponds to an average of 2.1 commissural macroconnections per region, their actual number varies over a broad range (input range 0–8; output range 0–13). All 96 identified commissural connections are in the very weak, weak, and weak to moderate weight categories. Twelve of 45 regions generated a homotopic commissural connection (to the same region on the contralateral side) and 84 of the commissural connections were heterotopic (to a different region on the contralateral side); all commissural connections were deemed symmetric with respect to the two sides because no evidence of right–left asymmetries was found.

A complete (both hemispheres) connection matrix for the cerebral nuclei is formed by the addition of commissural connections to the association connections (Fig. S5). Modules for the two-hemisphere (90-region) network were detected as for the single hemisphere, by varying the resolution parameter. By far the most stable solution contained eight modules, four in each hemisphere, matching the four-module solution found in the single-hemisphere analysis (Fig. 7).

The density and weight of commissural connections by modules are summarized in Table S3 and a layout of the network for the two hemispheres is shown in Fig. 8. Module M1 maintains no commissural connections, whereas in contrast, M2 generates by far the most commissural connections, particularly with M2 and M3. Within modules M2–M4, regions BSTam, BSTdm, BSTal, BSTrh, and fusiform nucleus of bed nuclei of terminal stria (BSTfu) maintain the most commissural connections. The extent and distribution of association and commissural connections arising in one hemisphere is clearly illustrated by removing the association and commissural connections arising in the other hemisphere from the fully bilateral network (Fig. 9; compare with Fig. 8).

The number of intrahemispheric connections maintained by each region strongly correlates with the number of its commissural connections (Fig. 10). Computing the shortest paths for the 90-region network reveals that paths connecting modules across the two hemispheres vary greatly in length. M4(side1 ↔ side2) is linked by relatively short paths, whereas paths between M1(side1 ↔ side2) are among the longest in the entire network.

Inclusion of commissural connections (and inclusion of communication paths that span the two hemispheres) results in changed hub score rankings. Regions BSTal, BSTrh, and

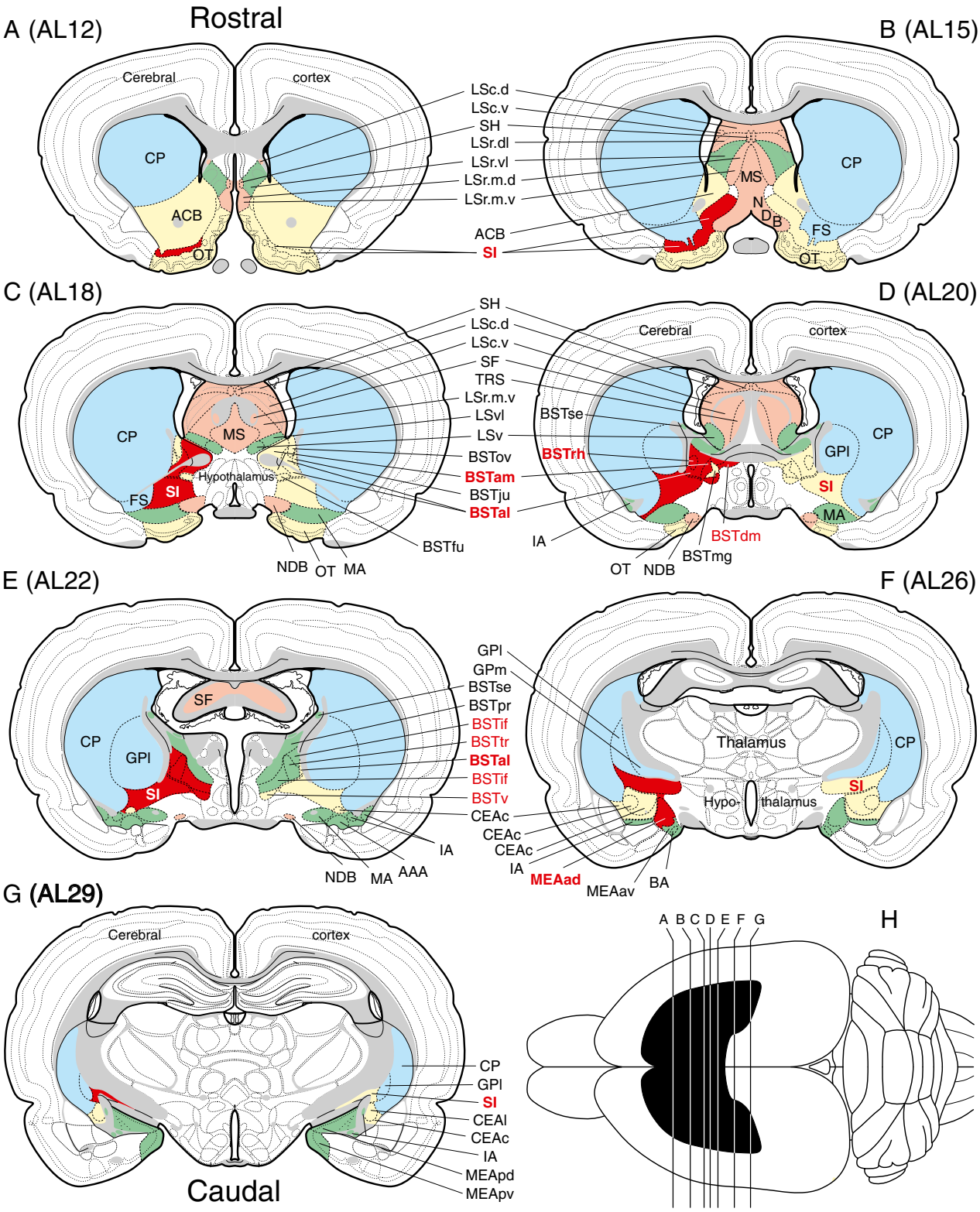

Fig. 6. Topographic distribution of modules and rich club. Regions, modules, and rich club are plotted on a standard atlas of the rat brain (16), with atlas levels (AL in *A*–*G*) arranged from rostral to caudal, as indicated in the dorsal view of the rat brain (*H*). For clarity, the rich club (red) is shown only on the left side of the brain. Modules are color coded as in Figs. 5 and 8; for abbreviations see Fig. 1.

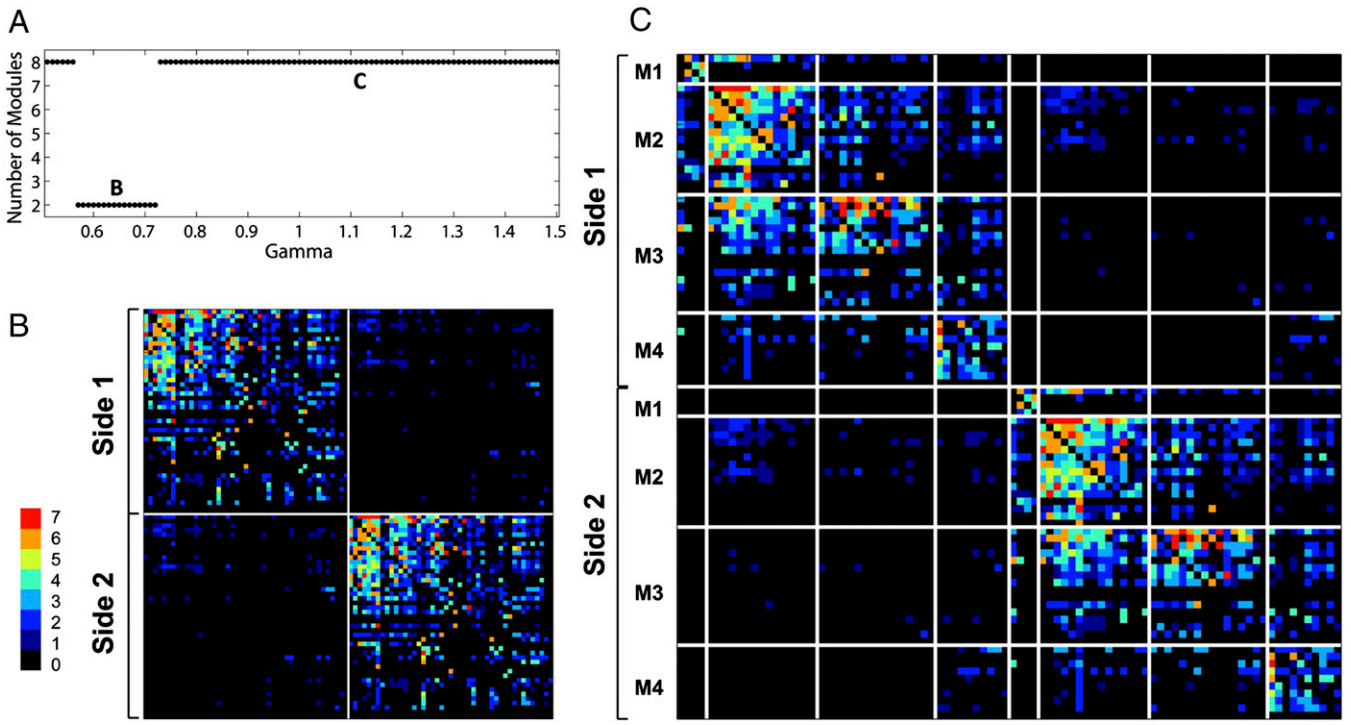

Fig. 7. Module stability for connections between the cerebral nuclei in each hemisphere, displayed here for the bihemispheric 90-region network. *A* shows the number of modules, and *B* and *C* show stable module partitions encountered in the range $\gamma = [0.5–1.5]$, with regions within modules arranged by their total node strength. One partition into $4 + 4$ modules (identical to that in Fig. 3*A*) remains stable across most of the parameter range. Regions in *C* are arranged in the same order as for Fig. 3*A*, in both hemispheres.

MEAad maintain their status as putative hubs with 80th percentile rankings in all four centrality measures (degree, strength, betweenness, closeness), whereas regions SI and BSTam drop out.

Discussion

This study yielded four basic results. First, the intracerebral nuclei network is arranged in four asymmetrically interconnected and topographically distinct network modules based on number

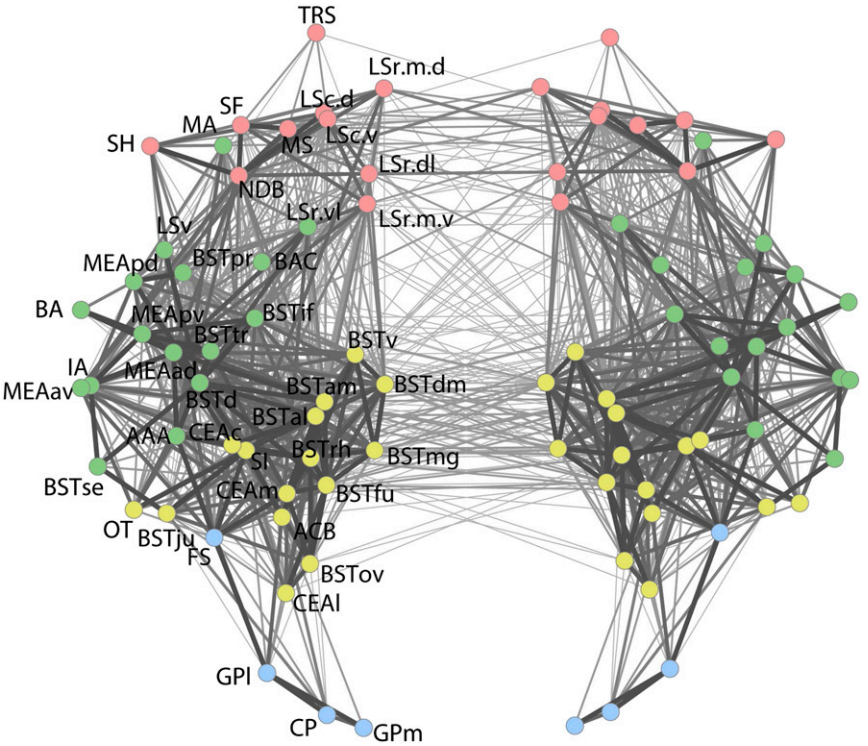

Fig. 8. Layout for the 90-region network between the cerebral nuclei regions on both sides of the brain. Methodology and all conventions are as in Fig. 5*A*. Region (node) labels are shown only for side 1 (*Left*), and region positions are symmetric across the midline, with homotopic connections extending horizontally as they connect symmetrically arranged node pairs on the two sides.

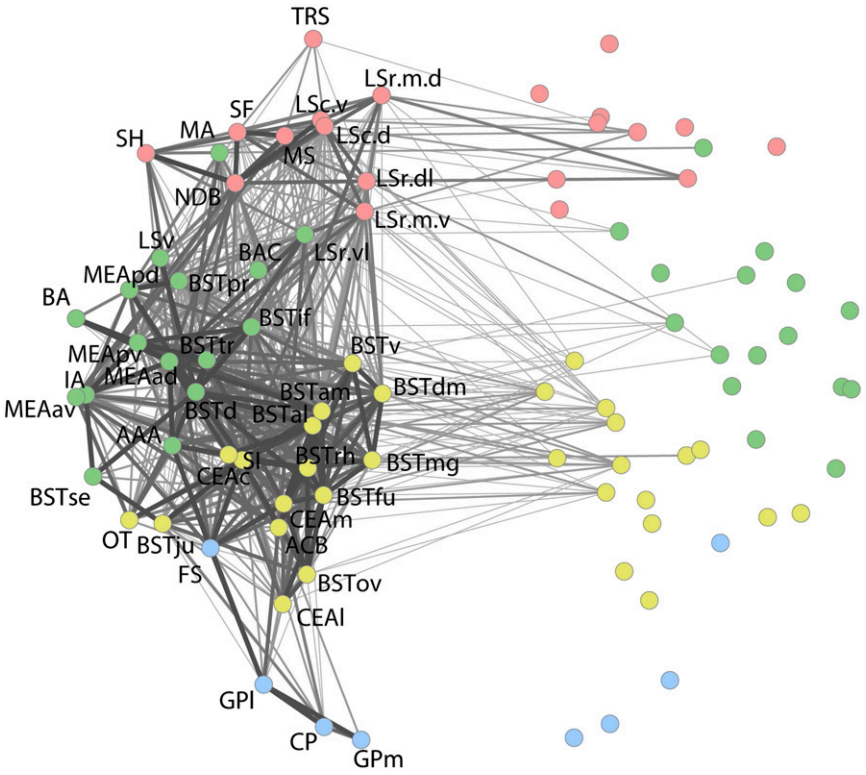

Fig. 9. Layout for association (*Left*) and commissural (*Right*) connections originating from the 45 cerebral nuclei regions in one hemisphere. Association and commissural connections originating from the cerebral nuclei regions in the other hemisphere are assumed to be symmetric in rat (Fig. 8) based on current data. All conventions are as in Figs. 5*A* and 8.

and weight of connections. Second, the association connection subnetwork is much denser than the commissural subnetwork. Third, a topographically continuous band of rich club and hub regions (nodes) stretches through two of the modules. And fourth, the network as a whole does not show small-world organization.

There are obvious similarities and differences between the rat cerebral nuclei association network described here and the rat cerebral cortical association network recently analyzed with similar methodology (10). Both networks are quite dense (in the sense that around 40% of all possible connections exist), both display four modules that are asymmetrically interconnected and topographically distinct, and both have a topographically segregated band of rich club and hub regions. The most striking difference is that the cortical association network shows much stronger expression of small-world attributes (specifically short path length conferring high efficiency), which are not as clearly apparent in the cerebral nuclei association network. This finding was unexpected because small-world topology was a common feature in earlier analyses of nervous system organization, many of them carried out on representations of cortical networks (19).

Instead, the intracerebral nuclei network has several connectional characteristics that set it apart from previous cortico-cortical datasets, including the rat cerebral cortical association macroconnection network (10). For example, the network displays a lesser extent of reciprocity (that is, a greater tendency toward unidirectional or asymmetrically weighted connections), at the level of both individual nodes and network modules. This results in less direct communication patterns, longer path lengths, and lower global efficiency. Another major difference with important implications for network modeling is that the sign of most cerebral cortical association connections is presumably positive (excitatory) whereas the sign of most cerebral nuclei association connections is presumably negative (inhibitory) (3). These differences in architectural features may reflect differences in function, with the small-world topology of cortico-cortical networks promoting the integration of information (requiring globally short paths) whereas intracerebral nuclei networks mediate the flow of neural signals between cortex and subcortical regions involved in controlling specific behaviors (biased toward parallel and independent paths).

The structure–function significance of the four network modules in each hemisphere and the connections within and between modules (in both hemispheres; Fig. 7) are not immediately obvious. However, one generalization seems clear: Module M1 corresponds to the classical striatopallidum, which receives its major input from isocortex and is involved in somatomotor control mechanisms

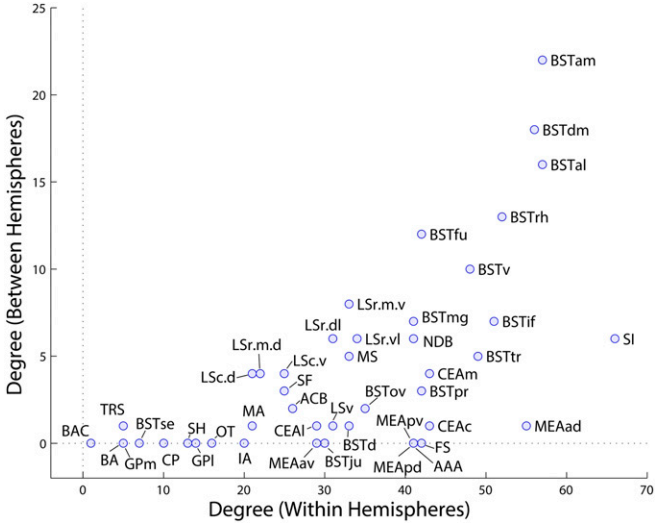

Fig. 10. Scatter plot of each region's intrahemisphere degree (the number of its distinct input plus output connections, absent any commissural connections) vs. the region's interhemisphere degree (the number of its distinct commissural connections, both homo- and heterotopic inputs plus outputs). The two measures are significantly correlated (Pearson correlation, $R = 0.619$, $P = 5.84 \times 10^{-6}$; Spearman correlation, $R = 0.641$, $P = 2.14 \times 10^{-6}$). For abbreviations see Fig. 1.

(3, 4), whereas the other three modules (M2–M4) receive their major input from limbic cortex and are involved in motivated behavioral mechanisms (4, 5, 7, 17, 18). As broad generalizations, module 2 contains the central amygdalar nucleus and anterior division of the bed nuclei of the terminal stria and has been most notably implicated in homeostatic behaviors (for example, eating and drinking) and anxiety (17, 20, 21, 22, 23); module 3 contains the medial amygdalar nucleus and posterior division of the bed nuclei of the terminal stria and has been implicated most notably in social interactions and responding to threats in the environment (17, 24, 25); and module 4 receives its major inputs from the hippocampus and may thus play a role in spatial and mnemonic influences on motivated behavior in general (18).

Furthermore, the nine members of the rich club (and the subset of putative hubs within it: SI, BSTam, BSTv, BSTdm, BSTal, BSTrh, BSTif, BSTtr, and MEAad) all reside in M2 and M3, and the extrinsic connections of the rich club predict that collectively they coordinate somatic, autonomic, and neuroendocrine responses in motivated survival behaviors, including reproductive, fight or flight, eating and drinking, and foraging (5, 20–25).

There are three main limitations of the present study. First, the analysis was based on macroconnections, that is, connections between one gray matter region and another. Macroconnectomics provide a high-level view of network design principles, but do not take into account the critical role of connections between distinct neuron types making up each gray matter region or the connections of individual neurons forming each neuron-type population. Relatively few systematic data currently exist for connections between neuron types and individual neurons in the mammalian cerebral nuclei, but our analysis provides a framework for interpreting future datasets at these deeper levels of analysis.

The second limitation is that the database used here is not complete. We did not identify data for ∼10% of all possible connections, and not all connection reports relied on the best available methodology; importantly, however, these gaps have been identified systematically. In addition, the results could vary with different parceling schemes for cerebral nuclei regionalization and with the addition of more accurate and reliable connection data. From a neuroinformatics perspective, this is simply version 1.0 of the rat intracerebral macroconnectome, and future versions can be easily computed from updated data in Dataset S3. Presumably results will vary in proportion to the magnitude of differences between versioned datasets, but it has been shown that, at least qualitatively, the results of modularity analysis become stable with adjacency matrix fill ratios greater than 60–70% (10).

The third main limitation of this study is that the macroconnectome assembled here examined only the organization of intrinsic circuitry between the 45 parts of the cerebral nuclei. The equally important extrinsic connections remain to be assembled for systematic network analysis. This project is underway but to understand fully the role of cerebral nuclei connectivity will require placing it within the context of the nervous system connectome as a whole, including its interactions with the rest of the body—the neurome.

Materials and Methods

Methods for the underlying network analysis are essentially the same as those described in detail elsewhere (10) and in *SI Materials and Methods*. All relevant data in the primary literature were interpreted in the only available standard, hierarchically organized, annotated nomenclature for the rat brain (Dataset S1), using descriptive nomenclature defined in the foundational model of connectivity (11, 12). Association and commissural connection reports were assigned ranked qualitative connection weights based on pathway tracing methodology, injection site location and extent, and anatomical density. All connection reports are provided in an Excel worksheet (Dataset S2), and the data used just to construct connection matrices are provided in another Excel worksheet (Dataset S3).

1. Herrick CJ (1910) The morphology of the forebrain in amphibia and reptilia. *J Comp Neurol Psychol* 20(5):413–547.
2. Alvarez-Bolado G, Swanson LW (1996) *Developmental Brain Maps: Structure of the Embryonic Rat Brain* (Elsevier, Amsterdam).
3. Nieuwenhuys R, Voogd J, van Huijzen C (2008) *The Human Central Nervous System* (Springer, Berlin), 4th Ed.
4. DeLong MR, Wichmann T (2015) Basal ganglia circuits as targets for neuromodulation in Parkinson disease. *JAMA Neurol* 72(11):1354–1360.
5. Heimer L, Wilson RD (1975) The subcortical projections of the allocortex: Similarities in the neural associations of the hippocampus, the piriform cortex, and the neocortex. *Golgi Centennial Symposium Proceedings*, ed Santini M (Raven, New York), pp 177–193.
6. de Olmos JS, Heimer L (1999) The concepts of the ventral striatopallidal system and extended amygdala. *Ann N Y Acad Sci* 877:1–32.
7. Swanson LW (2000) Cerebral hemisphere regulation of motivated behavior. *Brain Res* 886(1–2):113–164.
8. Rubinov M, Sporns O (2010) Complex network measures of brain connectivity: Uses and interpretations. *Neuroimage* 52(3):1059–1069.
9. Sporns O, Betzel RF (2016) Modular brain networks. *Annu Rev Psychol* 67:613–640.
10. Bota M, Sporns O, Swanson LW (2015) Architecture of the cerebral cortical association connectome underlying cognition. *Proc Natl Acad Sci USA* 112(16):E2093–E2101.
11. Swanson LW, Bota M (2010) Foundational model of structural connectivity in the nervous system with a schema for wiring diagrams, connectome, and basic plan architecture. *Proc Natl Acad Sci USA* 107(48):20610–20617.
12. Brown RA, Swanson LW (2013) Neural systems language: A formal modeling language for the systematic description, unambiguous communication, and automated digital curation of neural connectivity. *J Comp Neurol* 521(13):2889–2906.
13. Swanson LW, Lichtman JW (2016) From Cajal to connectome and beyond. *Annu Rev Neurosci* 39:197–216.
14. Fortunato S, Barthélemy M (2007) Resolution limit in community detection. *Proc Natl Acad Sci USA* 104(1):36–41.
15. Squartini T, Picciolo F, Ruzzenenti F, Garlaschelli D (2013) Reciprocity of weighted networks. *Sci Rep* 3:2729.
16. Swanson LW (2004) *Brain Maps: Structure of the Rat Brain. A Laboratory Guide with Printed and Electronic Templates for Data, Models and Schematics* (Elsevier, Amsterdam), 3rd Ed.
17. Dong H-W, Petrovich GD, Swanson LW (2001) Topography of projections from amygdala to bed nuclei of the stria terminalis. *Brain Res Brain Res Rev* 38(1–2): 192–246.
18. Risold PY, Swanson LW (1997) Connections of the rat lateral septal complex. *Brain Res Brain Res Rev* 24(2–3):115–195.
19. Bassett DS, Bullmore E (2006) Small-world brain networks. *Neuroscientist* 12(6): 512–523.
20. Dong HW, Swanson LW (2003) Projections from the rhomboid nucleus of the bed nuclei of the stria terminalis: Implications for cerebral hemisphere regulation of ingestive behaviors. *J Comp Neurol* 463(4):434–472.
21. Dong H-W, Swanson LW (2004) Organization of axonal projections from the anterolateral area of the bed nuclei of the stria terminalis. *J Comp Neurol* 468(2):277–298.
22. Dong H-W, Swanson LW (2006) Projections from bed nuclei of the stria terminalis, dorsomedial nucleus: Implications for cerebral hemisphere integration of neuroendocrine, autonomic, and drinking responses. *J Comp Neurol* 494(1):75–107.
23. Dong H-W, Swanson LW (2006) Projections from bed nuclei of the stria terminalis, anteromedial area: Cerebral hemisphere integration of neuroendocrine, autonomic, and behavioral aspects of energy balance. *J Comp Neurol* 494(1):142–178.
24. Canteras NS, Simerly RB, Swanson LW (1995) Organization of projections from the medial nucleus of the amygdala: A PHAL study in the rat. *J Comp Neurol* 360(2): 213–245.
25. Dong H-W, Swanson LW (2004) Projections from bed nuclei of the stria terminalis, posterior division: Implications for cerebral hemisphere regulation of defensive and reproductive behaviors. *J Comp Neurol* 471(4):396–433.
26. Swanson LW (2015) *Neuroanatomical Terminology: A Lexicon of Classical Origins and Historical Foundations* (Oxford Univ Press, Oxford).
27. Swanson LW (2003) *Brain Architecture: Understanding the Basic Plan* (Oxford Univ Press, Oxford).
28. International Commission on Zoological Nomenclature (1999) *International Code of Zoological Nomenclature* (International Trust for Zoological Nomenclature, London).
29. Blondel V, Guillaume JL, Lambiotte R, Lefebvre E (2008) Fast unfolding of communities in large networks. *J Stat Mech* P10008.
30. Newman MEJ, Girvan M (2004) Finding and evaluating community structure in networks. *Phys Rev E Stat Nonlin Soft Matter Phys* 69(2 Pt 2):026113.
31. Maslov S, Sneppen K (2002) Specificity and stability in topology of protein networks. *Science* 296(5569):910–913.
32. Sporns O, Honey CJ, Kötter R (2007) Identification and classification of hubs in brain networks. *PLoS One* 2(10):e1049.
33. Harriger L, van den Heuvel MP, Sporns O (2012) Rich club organization of macaque cerebral cortex and its role in network communication. *PLoS One* 7(9):e46497.
34. Colizza V, Flammini A, Serrano MA, Vespignani A (2006) Detecting rich-club ordering in complex networks. *Nat Phys* 2:110–115.
35. Benjamini Y, Hochberg Y (1995) Controlling the false discovery rate: A practical and powerful approach to multiple testing. *J R Stat Soc B* 57:289–300.

Supporting Information

Swanson et al. 10.1073/pnas.1613184113

SI Materials and Methods

Cerebral Nuclei Histological Parcellation Granularity. To facilitate comparative analysis of rat connection data, they were collated with reference to a standard rat brain atlas (16), but with gray matter regions of the rat central nervous system (CNS) arranged with respect to a CNS hierarchical nomenclature in a strictly topographic order as outlined elsewhere (26), rather than in a structure–function order followed earlier (10, 16, 27). In addition, the CNS hierarchical levels of gray matter regions and subregions were explicitly recognized as comparable (respectively) to the species and subspecies levels in animal taxonomy (28) (Dataset S1). This nomenclature scheme recognizes 45 gray matter regions in the rat cerebral nuclei, all of which are included in the present analysis.

Connection Report Collation and Selection for Network Analysis. Our methodology for expertly collating connectional data from the primary neuroanatomical research literature was described in detail previously (10) and is summarized here. First, the primary literature was searched to find the best available connection data, from which connection reports were created. Several criteria were used to assess the quality of connection data: These included the validity of the experimental pathway tracing method used, restriction of the pathway tracer injection site to the gray matter region of interest, injection site coverage of the region of interest, and thoroughness of description of the connection. Next, for each possible connection in the connectome for which data were available, a single connection report was selected as best representative of the connection (using the criteria noted above). If more than one connection report was created for a given connection (depending on the availability of data in the primary literature), then, all else being equal, the connection report with the highest connection weight was selected. Finally, the weight of each selected connection report was used to populate a connection matrix that was used for subsequent network analysis.

The process of collation was considerably aided by the use of a dedicated data entry platform (Axiome; created by J.D.H.) designed as a spreadsheet template for use with Microsoft Excel. The template facilitates speed and accuracy of data entry by using data validation and conditional formatting rules and a highly structured and guided user-friendly interface. The complete set of connection report data used in the present analysis is available in Dataset S2.

Connection Weight Scaling Methodology for Network Analysis. There are almost no quantitative data available in the literature for the rat macroconnections used in this analysis. Therefore, ranked qualitative connection weights from the literature were divided into 12 value categories. In ascending order, they are no data, unclear, absent, axons of passage, very weak, weak, weak to moderate, present (value unreported), moderate, moderate to strong, strong, and very strong. For the purposes of our network analysis, reports of axons of passage were assigned a weight of "weak," and connections for which the reported value was entered as "present" (weight unreported) were assigned a weight of "moderate." When network analysis was applied to the dataset, the category values of unclear and no data were assigned to the absent category. Thus, the set of ranked qualitative values used for network analysis included 8 values (7 weights and 0 for absent) that were considered for our purposes to form an ordinal scale. As justified previously (10), the ranked qualitative connection weights were then transformed to approximately logarithmically spaced weights for network analysis, using a 10^4 exponential scale.

Network Analysis Methods. Network analyses were carried out on the directed and log-weighted rat intracerebral nuclei macroconnection (RiCNM) matrix (Figs. 1 and 4 and Fig. S4), using tools collected in the Brain Connectivity Toolbox (www.brain-connectivity-toolbox.net). Detailed descriptions of most network measures can be found in ref. 8. Rat cerebral nuclei gray matter regions are referred to as nodes of the RiCNM network.

For detection of optimal module partitions we implemented the Louvain algorithm (29) for modularity maximization (9, 30), including a resolution parameter γ designed to address a known limitation of modularity optimization, the resolution limit (14). Varying γ effectively allows the detection of modules that range over several spatial scales. In our study, the parameter γ was varied over a range of $\gamma = [0.5–1.5]$, an interval centered on the default setting of $\gamma = 1$; higher and lower settings of γ yielded mostly unstable solutions with unrealistically low or high numbers of modules. Robust module partitions are expected to remain stable over a broad range of settings of γ; that is, they should be insensitive to small variations in spatial scale. We optimized modularity 1,000 times for each setting of γ and encountered very little degeneracy in the distribution of solutions across these 1,000 iterations. Hence we selected the globally optimal module partition at each level of γ for further analysis.

Analyses of global network metrics such as clustering and efficiency, reciprocity, and rich club organization were statistically evaluated by comparison with a degree-sequence–preserving distribution of null models, as in previous work (10). Rewiring of the networks composing the random null model followed a commonly used procedure equivalent to a Markov switching algorithm (31) that preserves the number of incoming and outgoing connections on all nodes.

As in previous work (10, 32, 33), network hubs were determined on the basis of aggregated rankings across several distinct nodal centrality measures. These measures were node degree, node strength, node betweenness centrality, and closeness centrality. The node degree is defined as the sum of all incoming and outgoing connections per node. The node strength is defined as the total weight of all incoming and outgoing connections per node (computed from the weighted connection matrix). The node betweenness expresses the fraction of shortest paths that pass through each node. Closeness was calculated as the average of the row and column sum of the network's distance matrix. Betweenness and closeness were both derived from the weighted connection matrix, after converting connection weights to lengths, using an inverse transform. After ranking nodes on each of the four metrics, an aggregate "hub score" was determined for each node, expressing the number of metrics for which each node appeared in the top 20% (top nine nodes).

Rich club organization refers to a simple property that is shared by many, but not all, complex biological networks (34)—the propensity of highly connected nodes (that is, nodes with high degree) to also be densely connected to each other, more so than expected by chance. Our analysis proceeded along the following steps, in line with previous work (10). First, for each value of node degree k, the total sum of the weights $W_{>k}$ between all nodes with degree k or higher was determined. No distinction is made between incoming and outgoing connection weights. Next, the weighted rich club coefficient $\Phi^w(k)$ was computed as the ratio between $W_{>k}$ and the sum of the weights of the strongest

$E_{>k}$ connections across the whole network. The weighted rich club coefficient was then normalized against a set of 10,000 randomly rewired networks, preserving network size, density, and degree sequence (see above). Comparison of the rich club coefficient of the empirical network to this random null distribution was then subjected to significance testing. To correct for multiple comparisons over the range of degrees k examined, false-discovery rate correction was performed (35), at a false discovery rate of 0.001.

Reciprocity was assessed following the approach by Squartini et al. (15). Briefly, the network was decomposed into a symmetric (reciprocated) part and an asymmetric (nonreciprocated) part. The weighted reciprocity of the network was then computed as the ratio between the total reciprocated weight (the sum of all of the weights contained in the reciprocated part) and the total weight of the network. This quantity was then scaled relative to the average weighted reciprocity derived from the degree-sequence–preserving random null model (see above). The resulting metric ρ indicates the tendency of the network to reciprocate ($\rho > 0$) or to avoid reciprocation ($\rho < 0$). In the case of $\rho > 0$, a higher value of ρ indicates a stronger tendency to reciprocate.

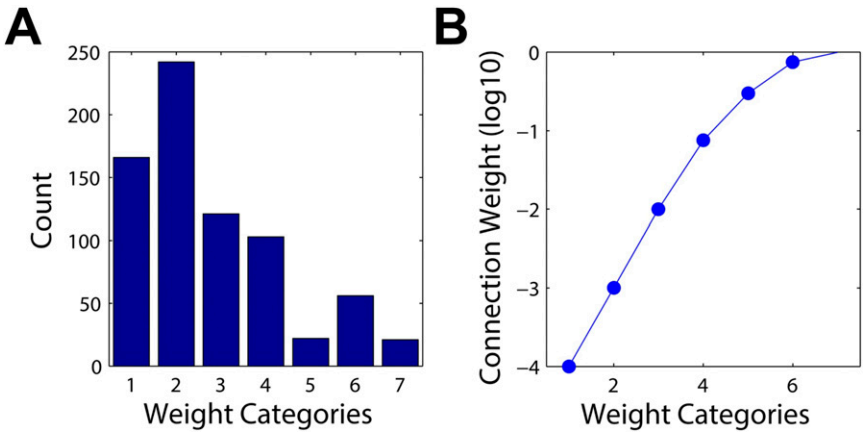

Fig. S1. (*A* and *B*) Distribution of weight categories of ipsilateral macroconnections (*A*) and weight scale used for weighted network analysis (*B*).

Red = hub & rich club member, red = rich club member only

Module 1 (N = 4, dorsal module or column) Blue
Striatal fundus (FS)
Lateral globus pallidus (GPl)
Caudoputamen (CP)
Medial globus pallidus GPm

Module 2 (N = 15, ventral module or column) Yellow
Rhomboid nucleus of bed nuclei of terminal stria (BSTrh)
Fusiform nucleus of bed nuclei of terminal stria (BSTfu)
Anterolateral area of bed nuclei of terminal stria (BSTal)
Anteromedial area of bed nuclei of terminal stria (BSTam)
Medial part of central amygdalar nucleus (CEAm)
Innominate substance (SI)
Magnocellular nucleus of bed nuclei of terminal stria (BSTmg)
Dorsomedial nucleus of bed nuclei of terminal stria (BSTdm)
Ventral nucleus of bed nuclei of terminal stria (BSTv)
Capsular part of central amygdalar nucleus (CEAc)
Oval nucleus of bed nuclei of terminal stria (BSTov)
Accumbens nucleus (ACB)
Juxtacapsular nucleus of bed nuclei of terminal stria (BSTju)
Lateral part of central amygdalar nucleus (CEAl)
Olfactory tubercle (OT)

Module 3 (N = 16, rostrocaudal module or column) Green
Anterodorsal part of medial amygdalar nucleus (MEAad)
Dorsal nucleus of bed nuclei of terminal stria (BSTd)
Posteroventral part of medial amygdalar nucleus (MEApv)
Transverse nucleus of bed nuclei of terminal stria (BSTtr)
Anterior amygdalar area (AAA)
Interfascicular nucleus of bed nuclei of terminal stria (BSTif)
Posterodorsal part of medial amygdalar nucleus (MEApd)
Anteroventral part of medial amygdalar nucleus (MEAav)
Stria extension of bed nuclei of stria terminalis (BSTse)
Bed nucleus of accessory olfactory tract (BA)
Principal nucleus of bed nuclei of terminal stria (BSTpr)
Intercalated amygdalar nuclei (IA)
Ventrolateral zone of rostral part of lateral septal nucleus (LSr.vl)
Ventral part of lateral septal nucleus (LSv)
Magnocellular nucleus (MA)
Bed nucleus of anterior commissure (BAC)

Module 4 (N =10, medial module or column) Red
Diagonal band nucleus (NDB)
Septofimbrial nucleus (SF)
Septohippocampal nucleus (SH)
Medial septal nucleus (MS)
Dorsal zone of caudal part of lateral septal nucleus (LSc.d)
Ventral region of medial zone of rostral part of lateral septal nucleus (LSr.m.v)
Ventral zone of caudal part of lateral septal nucleus (LSc.v)
Dorsal region of medial zone of rostral part of lateral septal nucleus (LSr.m.d)
Dorsolateral zone of rostral part of lateral septal nucleus (LSr.dl)
Triangular septal nucleus (TRS)

Fig. S2. Regional composition of the four modules displayed in Figs. 4, 5, 8, and 9.

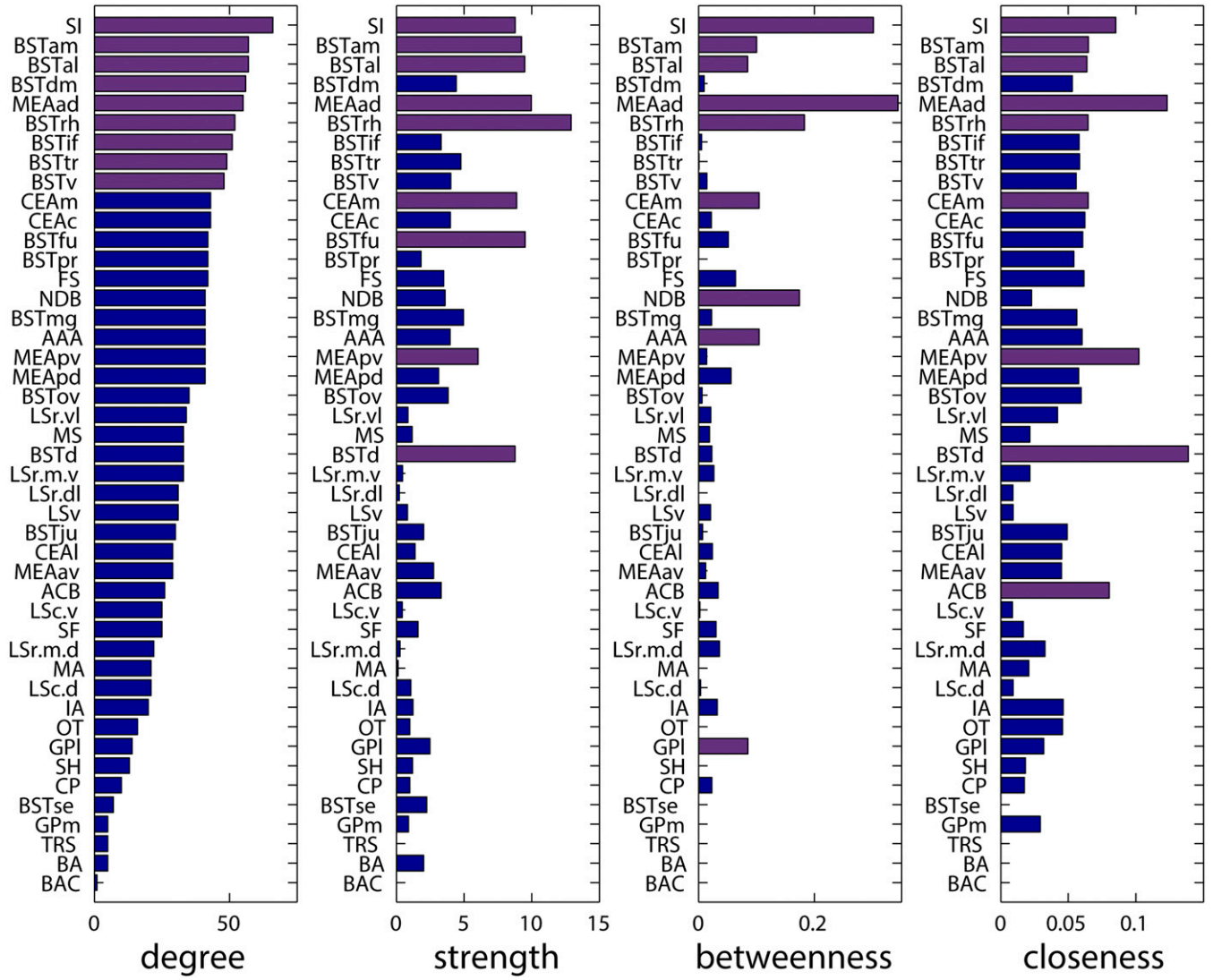

Fig. S3. Rankings of regions according to four centrality measures: degree, strength, betweenness, and closeness. Regions are ranked by degree across all four plots, with the top 20th percentile for each measure colored in purple.

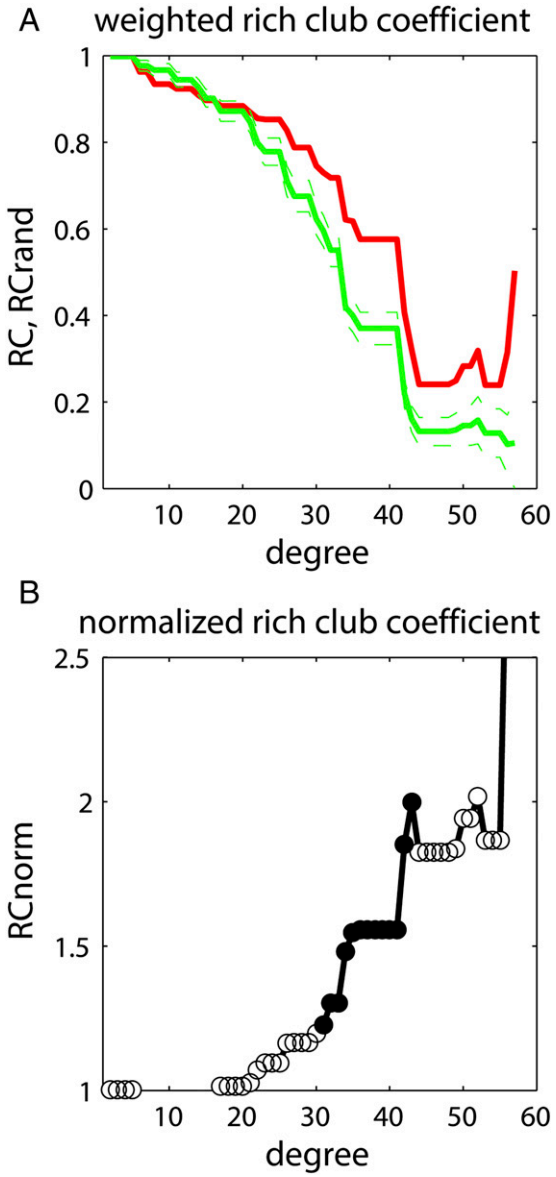

Fig. S4. Rich club organization. (*A*) Plots of the weighted rich club coefficient of the empirical network (red curve) and the mean (green curve) and mean ± SD (dashed green curves) for a population of randomized networks. (*B*) Normalized rich club coefficient across node degree, with statistically significant (after false discovery rate correction) data points shown in black.

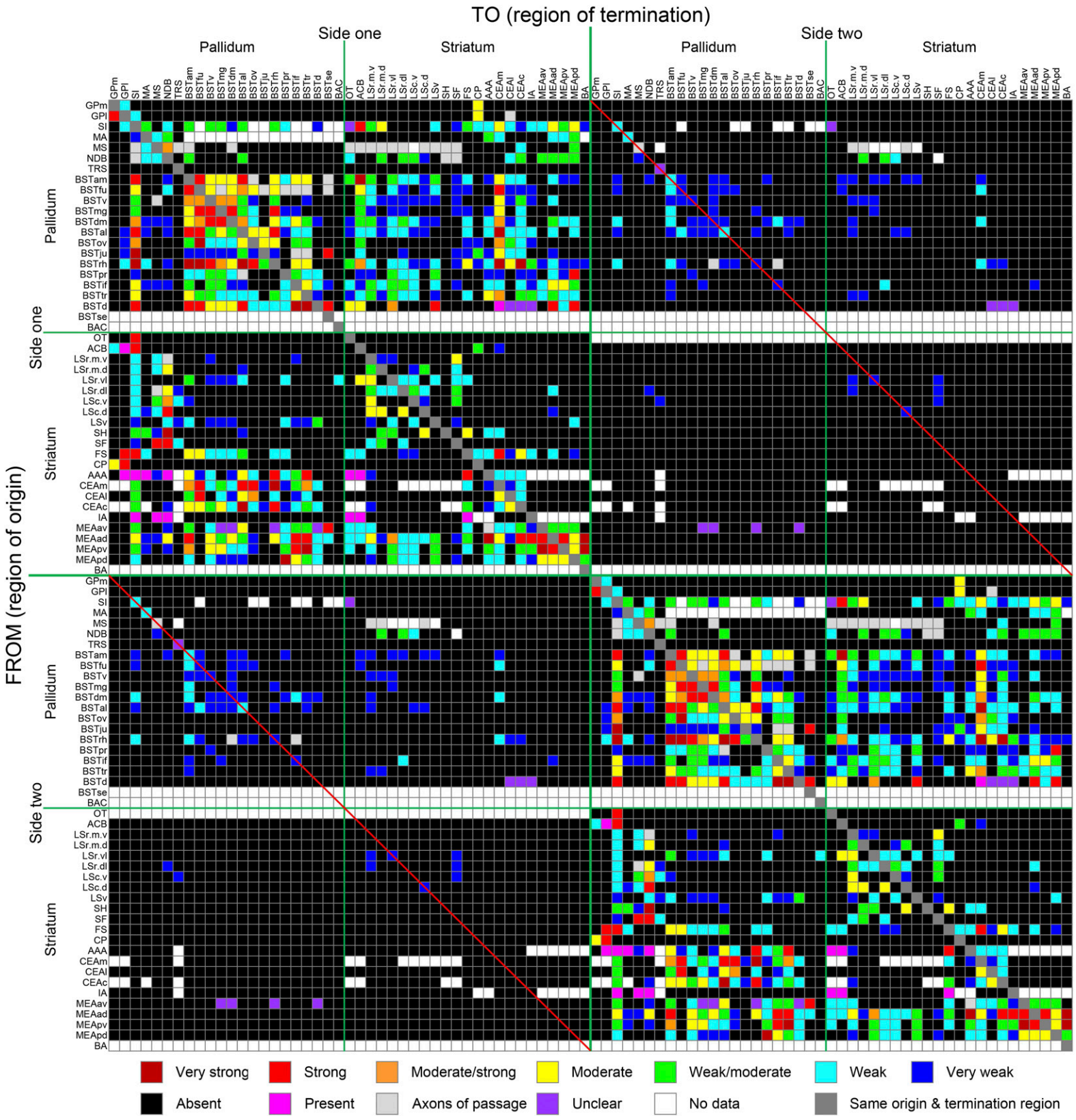

Fig. S5. Rat intracerebral nuclei connectome. Directed synaptic macroconnectome matrix with gray matter region sequence (*Left*, *Top* to *Bottom*, list of macroconnection origins/from; *Top*, *Left* to *Right*, same list of macroconnection terminations/to) in the Brain Maps 4 (Dataset S1) topographic nomenclature hierarchy. Ipsilateral connections are shown in *Upper Left* and *Lower Right Quadrants*, whereas contralateral connections are shown in *Upper Right* and *Lower Left Quadrants*. The red diagonal lines show homotopic commissural connections, that is, a connection arising from a region of interest on one side and terminating in the same region of interest on the other side. Use of these values for network analysis is described in *SI Materials and Methods*; for abbreviations see Fig. 1.

Table S1. Association connection density by module (binary and weighted)

	To			
From	M1	M2	M3	M4
Binary				
M1	0.6667	0.2500	0.0938	0.0500
M2	0.3833	0.7762	0.3708	0.3200
M3	0.1250	0.4833	0.4500	0.3000
M4	0.0250	0.1600	0.1125	0.6000
Weighted				
M1	0.2064	0.0291	0.0001	0.0000
M2	0.0033	0.1808	0.0072	0.0009
M3	0.0143	0.0334	0.0846	0.0032
M4	0.0019	0.0004	0.0005	0.0510

Table S2. Association connection weight categories by module (counts and percentages)

Connection	vw	w	w/m	m	m/s	s	vs
Counts							
M1 ↔ M1	0	2	0	3	0	3	0
M1 → M2	1	8	1	3	0	2	0
M1 → M3	1	5	0	0	0	0	0
M1 → M4	2	0	0	0	0	0	0
M2 → M1	9	8	4	2	0	0	0
M2 ↔ M2	21	29	29	32	15	25	12
M2 → M3	31	38	11	7	1	1	0
M2 → M4	31	12	4	1	0	0	0
M3 → M1	0	4	1	2	0	1	0
M3 → M2	24	40	17	26	2	7	0
M3 ↔ M3	14	31	27	12	2	14	8
M3 → M4	17	21	4	6	0	0	0
M4 → M1	0	0	0	1	0	0	0
M4 → M2	5	15	4	0	0	0	0
M4 → M3	4	7	7	0	0	0	0
M4 ↔ M4	6	22	12	8	2	3	1
%							
M1 ↔ M1	0	25	0	38	0	38	0
M1 → M2	7	53	7	20	0	13	0
M1 → M3	17	83	0	0	0	0	0
M1 → M4	100	0	0	0	0	0	0
M2 → M1	39	35	17	9	0	0	0
M2 ↔ M2	13	18	18	20	9	15	7
M2 → M3	35	43	12	8	1	1	0
M2 → M4	65	25	8	2	0	0	0
M3 → M1	0	50	13	25	0	13	0
M3 → M2	21	34	15	22	2	6	0
M3 ↔ M3	13	29	25	11	2	13	7
M3 → M4	35	44	8	13	0	0	0
M4 → M1	0	0	0	100	0	0	0
M4 → M2	21	63	17	0	0	0	0
M4 → M3	22	39	39	0	0	0	0
M4 ↔ M4	11	41	22	15	4	6	2

m, moderate; m/s, moderate/strong; s, strong; vs, very strong; vw, very weak; w, weak; w/m, weak/moderate.

Table S3. Commissural connection density by module (binary and weighted)

	To side 1			
From side 2	M1	M2	M3	M4
Binary				
M1	0	0	0	0
M2	0	0.1952	0.0458	0.0667
M3	0	0.0167	0.0042	0.0313
M4	0	0	0	0.1333
Weighted $\times 10^{-3}$				
M1	0	0	0	0
M2	0	0.0667	0.0121	0.0067
M3	0	0.0017	0.0004	0.0087
M4	0	0	0	0.2733

Dataset S1. Brain Maps 4 annotated nomenclature table

Dataset S1

This is a rearrangement of the cerebral nuclei parts in table B of Brain Maps 3 (16), with updated annotations as endnotes. The nomenclature hierarchy in Brain Maps 3 was arranged according to a structure–function model of the central nervous system (27). The nomenclature in this beta version of Brain Maps 4 is arranged according to a strictly topographic model of the central nervous system documented elsewhere (ref. 26, Dataset S3), as adapted for the rat, with region-level terms highlighted in red and subregion-level terms under them italicized.

Dataset S2. The complete collated connection report dataset used for network analysis

Dataset S2

The sequence of tabulated connection reports follows the list of regions in Dataset S1. When multiple connection reports for a connection of interest were found, one was chosen for network analysis (as described in *SI Materials and Methods*), with a selected value of "yes" (those that were not chosen are listed at the end of the table). Abbreviations for pathway tracers: ARGM, autoradiographic method; BDA-10K, biotinylated dextran amine, M_r 10,000); BDA-3K, biotinylated dextran amine, M_r 3,000); CTB, cholera toxin B subunit; Fluoro-Gold; HRP, horseradish peroxidase; neurobiotin; PHAL, *Phaseolus vulgaris* leucoagglutinin; True Blue; WGA-HRP, horseradish peroxidase conjugated to wheat germ agglutinin.

Dataset S3. Data matrices in Microsoft Excel workbook (spreadsheet) format for the association and commissural connections of the rat cerebral nuclei derived from collation of connection reports from the primary literature (as described in this article)

Dataset S3

The workbook has four matrices, each on a separate worksheet: (*i*) CN 1–1 binned and (*ii*) CN 1–2 binned [respectively, cerebral nuclei (CN) association and commissural connection matrices with connection weights represented on an ordinal 0–7 scale—these data were used for modularity analysis] and (*iii*) CN 1–1 raw and (*iv*) CN 1–2 raw (respectively, CN association and commissural connection matrices based on connection reported values and represented as weights on an ordinal 0–12 scale). A fifth worksheet (Key) provides descriptors for reported values and correspondence between raw and binned weights. Connection matrix directionality is from *y* axis to *x* axis. For abbreviations see Fig. 1.